Surface structure and hole localization in bismuth vanadate: A first principles study

Kyoung E. Kweon and Gyeong S. Hwang

Additional information on Appl. Phys. Lett.

Surface structure and hole localization in bismuth vanadate: A first principles study

Kyoung E. Kweon and Gyeong S. Hwang[a)]

Department of Chemical Engineering, University of Texas at Austin, Austin, Texas 78712, USA

The monoclinic and tetragonal phases of bismuth vanadate ($BiVO_4$) have been found to exhibit significantly different photocatalytic activities for water splitting. To assess a possible surface effect on the phase-dependent behavior, we calculate and compare the geometries and electronic structures of the monoclinic and tetragonal $BiVO_4$ (001) surfaces using hybrid density functional theory. The relaxed atomic configurations of these two surfaces are found to be nearly identical, while an excess hole shows a relatively stronger tendency to localize at the surface than the bulk in both phases. Possible factors for the phase-dependent photocatalytic activity of $BiVO_4$ are discussed. © *2013 AIP Publishing LLC*. [http://dx.doi.org/10.1063/1.4822270]

Bismuth vanadate ($BiVO_4$) has recently been recognized as a promising visible-light active photocatalyst for water splitting.[1–11] Interestingly, the photocatalytic activity has been found to be significantly enhanced in the monoclinic phase (ms-$BiVO_4$) in comparison to the tetragonal phase (ts-$BiVO_4$), although the two phases exhibit similar band structures.[1–3] While the underlying mechanisms are uncertain, a recent theoretical study[12] has demonstrated that a relatively weakly localized hole in ms-$BiVO_4$ may undergo faster diffusion than a small hole polaron in ts-$BiVO_4$, which may in turn facilitate hole transport to the surface and thus water oxidation reaction. Such hole mobility difference can play a critical role in the phase-dependent photocatalytic activity of $BiVO_4$, but other possible factors may also need to be examined to clarify the intriguing behavior. In particular, it would be instructive to examine the surface atomic structure and electronic states of ts-$BiVO_4$ and ms-$BiVO_4$ and possible surface effects on the photocatalytic activity difference, as photocatalysis is often sensitive to the surface properties.[13–17]

In this letter, we examine and compare the surface geometries and electronic structures of ts-$BiVO_4$ and ms-$BiVO_4$ using hybrid density functional theory (DFT) calculations. Here, we only consider the (001) surface, which tends to have the lowest energy[18] and has also been shown to be the most important facet for photocatalysis.[15–17] We also examine the characteristics of hole trapping in the near-surface region with comparisons to those in the bulk. Based on the results, we discuss possible surface effects on the photocatalytic activity difference between ts-$BiVO_4$ and ms-$BiVO_4$.

While there is no noticeable difference in the surface properties, our study shows that the hole formation energy difference between at the (001) surface and in the bulk is about 0.1 eV larger in the monoclinic phase compared to the tetragonal phase due to their distinctly different bulk characteristics. The larger hole formation energy difference, along with the higher hole mobility as predicted by our previous study, in the monoclinic phase may contribute to some degree to facilitating the transport of photogenerated holes to the surface and thus hole-catalyzed water splitting.

Spin-polarized DFT calculations were performed using the Vienna *Ab-initio* Simulation Package (VASP 5.2.2).[19] We used the Perdew-Burke-Ernzerhof (PBE) exchange-correlation (xc) functional[20] with 25% Hartree-Fock (HF) exchange; here, the slowly decaying long-range part of the HF interaction was excluded following the Heyd–Scuseria–Ernzerhof (HSE) screened approach.[21] The PBE-HF25% xc functional has been found to reproduce well the structural properties of bulk ts-$BiVO_4$ and ms-$BiVO_4$;[22] the calculated lattice parameters for ms-$BiVO_4$ and ts-$BiVO_4$ are $a = 5.183$ Å, $b = 5.074$ Å, $c = 11.711$ Å, and $\gamma = 90.36°$ ($a = b = 5.121$ Å, and $c = 11.647$ Å). Further details can be found in Ref. 22.

The (001) $BiVO_4$ surface was modeled using a periodic slab with a vacuum gap of 10 Å in the z direction (to separate the slab system from its periodic images). The atoms in the slab were allowed to fully relax until the residual forces on all the constituent atoms become smaller than 0.02 eV/Å. The projected augmented wave method[23] with a plane-wave basis set ($E_{cut} = 450$ eV) was employed. The Brillouin zone of the surface (1×1) unit cell was sampled using a gamma-centered ($2 \times 2 \times 1$) Monkhorst-Pack k-point mesh for geometry optimization, and the k-point mesh size was increased to ($4 \times 4 \times 1$) in refining the corresponding electronic structure.

For reference, we first briefly review the atomic and electronic structures of bulk ts-$BiVO_4$ and ms-$BiVO_4$. As illustrated in Fig. 1(a), the scheelite-type $BiVO_4$ structure consists of isolated VO_4 tetrahedra (in grey) that are corner-connected by BiO_8 dodecahedra (in purple). Figure 1(b) shows orbital-resolved density of states (DOS); in ts-$BiVO_4$, the top of the valence band (VB) is mainly composed of the Bi $6s$ and O $2p$ states, whereas there is an additional contribution of the Bi $6p$ state in ms-$BiVO_4$. For ms-$BiVO_4$, due to hybridization between the Bi $6s$ and $6p$ states, each BiO_8 dodecahedron is noticeably distorted with four different Bi-O bonds. On the other hand, a Bi atom in ts-$BiVO_4$ is located at the center position with two distinct Bi-O bonds [see inset of Fig. 1(b)]. Overall, predicted bulk structures with PBE-HF25% are in good agreement with experimental data.[24,25]

Next, we calculated the (001) $BiVO_4$ surface structures employing a slab with a lateral size of 1×1 unit cell and a thickness of 16 Bi layers, as illustrated in Fig. 2; the slab thickness was chosen sufficiently large such that the center region

---

[a)]Author to whom correspondence should be addressed. Electronic mail: gshwang@che.utexas.edu.
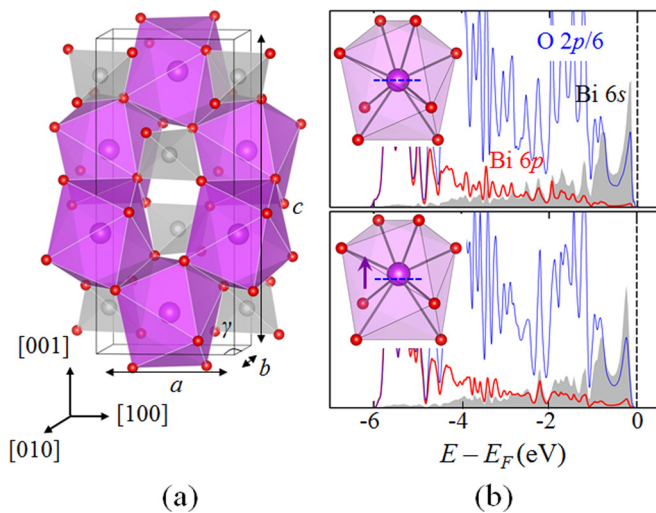
FIG. 1. (a) Crystal structure representation of scheelite $BiVO_4$ with indication of BiO_8 dodecahedra (in purple) and VO_4 tetrahedra (in gray) and (b) electron DOS projected onto the Bi $6s$ (shaded in gray), Bi $6p$ (red solid line), and O $2p$ (blue solid line) states in ts-$BiVO_4$ (upper panel) and ms-$BiVO_4$ (lower panel). In the DOS plots, the O $2p$ state is scaled by $1/6$ and the energy zero is set at the E_F which is indicated by the vertical dashed line. In the insets of (b), the geometries of a BiO_8 dodecahedron in ts-$BiVO_4$ (upper) and ms-$BiVO_4$ (lower) are shown; the arrow in ms-$BiVO_4$ represents a Bi displacement along the c-axis with respect to the corresponding center position in ts-$BiVO_4$ (indicated by a dotted line). Purple, silver, and red balls represent Bi, V, and O atoms, respectively.

(Bi8 and Bi8') exhibits the corresponding bulk-like structure. In the outmost surface layer, O (Bi) atoms have twofold (six fold) coordination, while bulk O (Bi) atoms are threefold (eight fold) coordinated; the under coordinated surface atoms
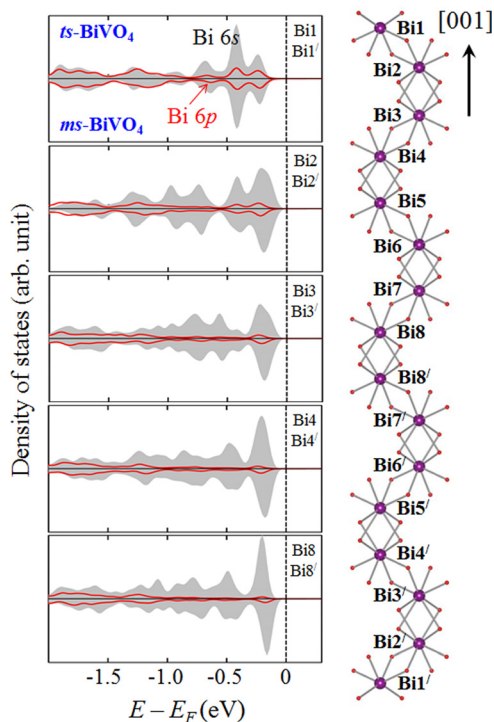

FIG. 2. (Left panels) DOS projected onto the $6s$ (shaded in gray) and $6p$ (red solid line) states of Bi atoms in the different layers of the ts-$BiVO_4$ (upper) and ms-$BiVO_4$ (lower) slabs. The energy zero is set at the E_F, which is indicated by the vertical dashed line. (Right panel) the geometry of the (001) $BiVO_4$ slab employed; only Bi and O atoms are shown for clarity (see Figure S1 in supplementary material for the complete slab structure[26]). Bin (or Bin') ($n = 1$–8) indicates the Bi atom in the nth subsurface Bi layer.

undergo rearrangements to minimize surface energy. (see Table S1 in supplementary material for the Bi-O bond lengths after surface relaxation for ts-$BiVO_4$ and ms-$BiVO_4$, together with the corresponding bulk values for comparison[26]).

For the ts-$BiVO_4$ surface, the outmost Bi atoms (Bi1/Bi1') are found to move inward by -0.13 Å along the [001] direction with respect to the unrelaxed structure, which in turn increases $d_{Bi-O}(1)$ while significantly reducing $d_{Bi-O}(2)$ and $d_{Bi-O}(3)$. Concurrently, the Bi atoms in the second (Bi2/Bi2') and third (Bi3/Bi3') subsurface layers are displaced outward by $+0.13$ Å and inward by -0.08 Å, respectively. As a result, the near-surface Bi atoms are no longer located at the BiO_8 polyhedron centers, unlike the bulk ts-$BiVO_4$ case. Further away from the surface, the surface-induced lattice distortions gradually diminish and the center region (Bi8/Bi8') becomes bulk-like. The relaxed ms-$BiVO_4$ surface shows a nearly identical structure to the ts-$BiVO_4$ surface. This is understandable given that surface relaxation is mainly driven by undercoordinated surface atoms; note that the two phases have the same atomic arrangement near surface. It may also be worth noting that the near-surface lattice relaxation is stronger than the monoclinic distortion in bulk ms-$BiVO_4$ (see Table S1 in supplementary material[26]).

With the optimized structures, we estimated the surface formation energies by $E_f = (E_{slab} - E_{bulk})/2A$, where E_{slab} and E_{bulk} are the total energies of the relaxed slab and bulk structures, respectively, A is the projected surface area, and the factor of 2 is introduced because the slab has two surfaces. The predicted E_f values for ts-$BiVO_4$ and ms-$BiVO_4$ are $0.30 \, J/m^2$ and $0.25 \, J/m^2$, respectively. We attribute the slightly larger E_f of ts-$BiVO_4$ to the relatively rigid nature of ts-$BiVO_4$ compared to ms-$BiVO_4$.[27] Notice also that the PBE-HF25% value of $E_f = 0.25 \, J/m^2$ for ms-$BiVO_4$ is considerably smaller than $0.50 \, J/m^2$ from previous DFT-PBE calculation.[18] This may imply that the $BiVO_4$ surface property prediction would be sensitive to the choice of xc functional; in fact, our recent studies[12,22] have demonstrated the strong xc functional dependence of monoclinic lattice distortion and charge localization/transport in bulk $BiVO_4$.

We further examined how the near-surface electronic structure changes in association with the surface relaxation, particularly Bi $6s$-$6p$ hybridization which is strongly related to local lattice distortions.[12,22,28,29] Figure 2 shows the DOS projected onto the Bi $6s$ and $6p$ orbitals at different subsurface layers. The DOS plots for the center region (indicated as Bi8/Bi8') are virtually identical to those of the bulk counterparts, reinforcing that the surface effect extends only a few layers deep. In the Bi1 layer, the $6p$ state is substantially pronounced near the Fermi level (E_F) ($-0.5 \, eV < E - E_f < 0$), indicating strong hybridization with the $6s$ state; the enhanced orbital overlap leads to the peak broadening and downshift. We also notice that there is almost no difference between the ts-$BiVO_4$ and ms-$BiVO_4$ cases, suggesting that the monoclinic and tetragonal phases may have similar surface electronic properties. The $6s$-$6p$ overlap is noticeably weakened in the Bi2 and Bi3 layers while ts-$BiVO_4$ and ms-$BiVO_4$ still show similarity. Below the Bi4 layer, the electronic structures for both phases become bulk-like.

The electronic structure variations near surface can be well demonstrated by the band-decomposed charge density
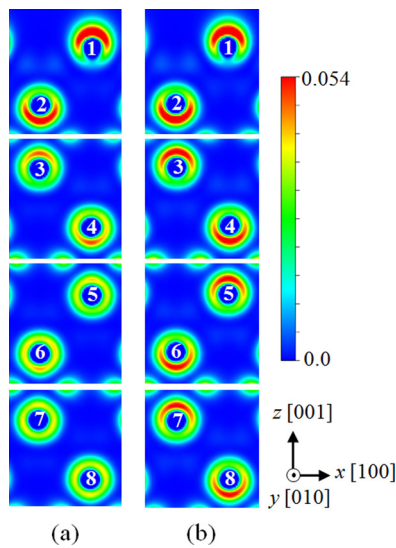
FIG. 3. Band-decomposed charge density within $-0.9\,\text{eV} < E - E_F < 0\,\text{eV}$ from the total DOS (not shown here) in (010) planes containing Bi atoms for the ts-BiVO$_4$ (a) and ms-BiVO$_4$ (b) slabs. Four Bi atoms (Bi1, Bi2, Bi5, and Bi6) are located on (010) plane at $y = 0.25$, while the other four Bi atoms (Bi3, Bi4, Bi7, and Bi8) are at $y = 0.75$. The unit of the color scale is e/Å^3. See Fig. 2 for the Bi atom labels.
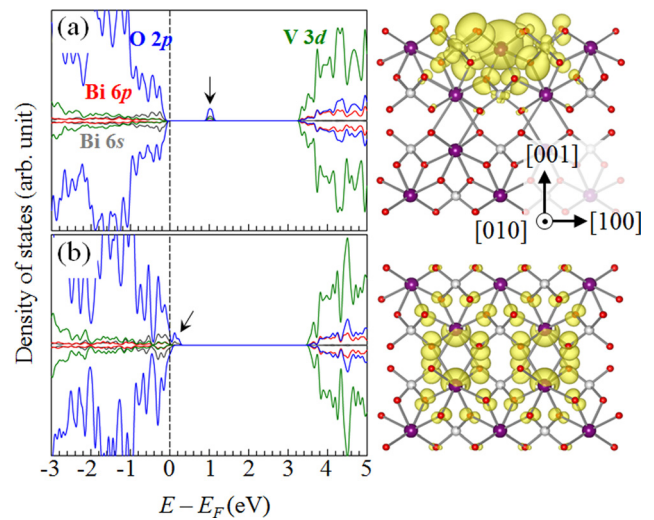

FIG. 4. (Left panels) Orbital projected DOS and (right panels) band-decomposed charge density for the polaronic (a) and nonpolaronic (b) hole states in the ms-BiVO$_4$ slab (with four Bi-layer thicknesses). In the DOS plots, the hole states are indicated by the arrows, and grey, red, green, and blue solid lines represent the Bi 6s, Bi 6p, V 3d, and O 2p states, respectively. The energy zero is set at the E_F which is indicated by the vertical dashed line. In the band-decomposed charge density plots, the isosurface value is 0.005 e/Å^3, and purple, silver, and red balls represent Bi, V, and O atoms, respectively.

plots shown in Fig. 3. In the near-surface region, the partial charge on Bi is asymmetrically distributed with a lobe aligned along the [001] in both phases, which are apparently attributed to the Bi 6s-6p hybrid state; the asymmetric Bi lone pair will be stereochemically active. In ts-BiVO$_4$, the charge distribution becomes nearly symmetric in the Bi5 layer and below, indicating that the Bi 6s lone pair is spherically symmetric with no significant interaction with the 6p state. On the other hand, in ms-BiVO$_4$ the Bi 6s lone pair likely remains stereochemically active in the deep subsurface layers, although the charge distribution becomes less asymmetric in comparison to the near-surface case.

Finally, we examined the behavior of an excess hole in the near-surface region employing a slab that consists of a 2×2 surface cell with four Bi layers; the slab's size turns out to be sufficiently large for the surface property study. The hole-doped system was constructed by removing one electron from the corresponding neutral system, while including a homogeneous background charge to maintain the overall charge neutrality of the charged supercell. We first created a localized (polaronic) hole state in the topmost Bi layer (by applying a small perturbation around a selected BiO$_6$ polyhedron to break the lattice symmetry prior to structural relaxation). Figure 4(a) shows the DOS for the polaronic hole state at the ms-BiVO$_4$ surface which lies about 1.2 eV above the top of the VB. The surface hole state tends to exist far deeper in the gap compared to the bulk hole state (which was found to lie only 0.6 eV above the top of the VB in ts-BiVO$_4$ or close to the VB edge in ms-BiVO$_4$).[12] This may suggest a relatively stronger tendency for holes to localize at the surface in comparison to the bulk. The hole charge is found to localize around the selected BiO$_6$ polyhedron, as demonstrated by the band-decomposed charge density plot in Fig. 4(a). The ts-BiVO$_4$ surface shows nearly identical features for hole localization, as expected; hence, not shown here. For both phases, about 22% of the hole charge is

predicted to reside on the outmost Bi site, and 49% is on the surrounding six O atoms; the rest spreads out beyond the BiO$_6$ region. The hole self-trapping is accompanied by local lattice distortions; there is noticeable shrinkage (by about 0.3 Å) in two Bi-O bonds with a minor change in other four Bi-O bonds, which can be attributed to the reduced Bi-O antibonding interaction associated with the charge depletion.[12,30]

We also assessed the relative stabilities of the polaronic states with respect to corresponding completely delocalized (nonpolaronic) states (which were obtained with no local perturbation[12]). As shown in Fig. 4(b), for the delocalized model of ms-BiVO$_4$, the Fermi level is shifted below the top of the VB, indicating hole creation in the VB. The corresponding band-decomposed charge density isosurface reveals that the hole spreads over Bi and O atoms in the subsurface layers. The nonpolaronic state with no local lattice distortion, as expected, has the almost same configuration as the neutral state structure. According to our PBE-HF25% calculations, the small polaronic state is predicted to be about 0.26 eV more favorable than the nonpolaronic state for both ms-BiVO$_4$ and ts-BiVO$_4$.

While the nearly identical surface structures of ms-BiVO$_4$ and ts-BiVO$_4$ are thought to exhibit similar hole-trapping characteristics, our previous hybrid DFT calculations showed distinctly different hole localization behaviors in the bulk phases.[12] That is, an excess hole tends to spread widely over many lattice sites (large polaron) in bulk ms-BiVO$_4$, whereas it localizes around a BiO$_8$ polyhedron with local lattice distortions (small polaron) in bulk ts-BiVO$_4$; the hole formation energy in ts-BiVO$_4$ is predicted to be about 0.1 eV lower than that in ms-BiVO$_4$. Such relatively more favorable hole formation in bulk ts-BiVO$_4$ may cause retardation in hole transport to the surface and thus suppression of hole-catalyzed water splitting to a certain

extent, in comparison to the ms-BiVO$_4$ case. As such, we think that the hole formation energy difference could be another (perhaps minor) factor that leads to the phase-dependent photocatalytic activity towards water splitting, in addition to the hole mobility difference between ms-BiVO$_4$ and ts-BiVO$_4$ as recently proposed.

In summary, DFT calculations using a hybrid (PBE-HF25%) xc functional were performed to examine BiVO$_4$ (001) surface properties. Upon relaxation, near-surface Bi atoms undergo displacements along the vertical [001] direction, while increasing the overlap of Bi 6s and 6p orbitals compared to the bulk counterparts. The surface relaxation effect tends to extend down to the third subsurface Bi layer, after which the bulk-like atomic and electronic structures are restored. Our hybrid DFT calculations show no noticeable difference between the reconstructed surface structures of the ms-BiVO$_4$ and ts-BiVO$_4$ phases. However, the surface formation energy of ts-BiVO$_4$ (=0.30 J/m^2) is predicted to be slightly larger than that of ms-BiVO$_4$ (=0.25 J/m^2), due to the relatively more rigid nature of bulk ts-BiVO$_4$ than ms-BiVO$_4$. An excess hole is found to localize on a surface Bi atom with local lattice distortions; the hole localization tendency appears to be stronger at the surface than the bulk. Although the hole-trapping characteristics at the ts-BiVO$_4$ and ms-BiVO$_4$ surfaces are nearly identical, in the bulk phase hole-doped ts-BiVO$_4$ tends to be more energetically favorable than the ms-BiVO$_4$ case. As a result, the hole formation energy difference between at the (001) surface and in the bulk is predicted to be about 0.1 eV larger in ms-BiVO$_4$ compared to ts-BiVO$_4$; the larger hole formation energy difference in the monoclinic phase may contribute to facilitating the transport of photogenerated holes to the surface and thus hole-catalyzed reactions at the surface to a certain degree. Based on the calculation results, we speculate that the hole formation energy difference could be another (perhaps minor) factor for the phase-dependent photocatalytic activity towards water splitting, in addition to the significant hole mobility difference between ms-BiVO$_4$ and ts-BiVO$_4$ as recently proposed. We would also like to point out that the degrees of surface relaxation and hole localization in aqueous environments would be different from those at the gas-solid interface; in fact, our preliminary calculations (not shown here) demonstrate that the presence of water tends to suppress the surface reconstruction and thus hole trapping, but not strong enough to alter the conclusions drawn from the present work.

[1]A. Kudo, K. Omori, and H. Kato, J. Am. Chem. Soc. **121**, 11459 (1999).

[2]S. Tokunaga, H. Kato, and A. Kudo, Chem. Mater. **13**, 4624 (2001).

[3]J. Yu and A. Kudo, Adv. Funct. Mater. **16**, 2163 (2006).

[4]S. Kohtani, S. Makino, A. Kudo, K. Tokumura, Y. Ishigaki, T. Matsunaga, O. Nikaido, K. Hayakawa, and R. Nakagaki, Chem. Lett. **31**, 660 (2002).

[5]M. Long, W. Cai, J. Cai, B. Zhou, X. Chai, and Y. Wu, J. Phys. Chem. B **110**, 20211 (2006).

[6]K. Sayama, A. Nomura, T. Arai, T. Sugita, R. Abe, M. Yanagida, T. Oi, Y. Iwasaki, Y. Abe, and H. Sugihara, J. Phys. Chem. B **110**, 11352 (2006).

[7]H. Luo, A. H. Mueller, T. M. McCleskey, A. K. Burrell, E. Bauer, and Q. X. Jia, J. Phys. Chem. C **112**, 6099 (2008).

[8]H. Ye, J. Lee, J. S. Jang, and A. J. Bard, J. Phys. Chem. C **114**, 13322–13328 (2010).

[9]H. S. Park, K. E. Kweon, H. Ye, E. Paek, G. S. Hwang, and A. J. Bard, J. Phys. Chem. C **115**, 17870 (2011).

[10]Y. Park, K. J. McDonald, and K. Choi, Chem. Soc. Rev. **42**, 2321 (2013).

[11]H. S. Park, K. C. Leonard, and A. J. Bard, J. Chem. Phys. C **117**, 12093 (2013).

[12]K. E. Kweon and G. S. Hwang, Phys. Rev. B **87**, 205202 (2013).

[13]G. Liu, J. C. Yu, G. Q. Lu, and H. M. Cheng, Chem. Commun. **47**, 6763 (2011).

[14]H. G. Yang, C. H. Sun, S. Z. Qiao, J. Zou, G. Liu, S. C. Smith, H. M. Cheng, and G. Q. Lu, Nature **453**, 638 (2008).

[15]D. Wang, H. Jiang, X. Zong, Q. Xu, Y. Ma, G. Li, and C. Li, Chem.-Eur. J. **17**, 1275 (2011).

[16]G. Xi and J. Ye, Chem. Commun. **46**, 1893 (2010).

[17]L. Zhang, D. Chen, and X. Jiao, J. Phys. Chem. B **110**, 2668 (2006).

[18]Z. Zhao, Z. Li, and Z. Zou, RSC Adv. **1**, 874 (2011).

[19]G. Kresse and J. Furthmuller, *VASP: The Guide* (Vienna University of Technology, Vienna, Austria, 2001).

[20]J. P. Perdew, K. Burke, and M. Ernzerhof, Phys. Rev. Lett. **77**, 3865 (1996).

[21]J. Heyd, G. E. Scuseria, and M. Ernzerhof, J. Chem. Phys. **118**, 8207 (2003).

[22]K. E. Kweon and G. S. Hwang, Phys. Rev. B **86**, 165209 (2012).

[23]P. E. Blochl, Phys. Rev. B **50**, 17953 (1994).

[24]A. W. Sleight, H.-Y. Chen, and A. Ferretti, Mater. Res. Bull. **14**, 1571 (1979).

[25]W. I. F. David and I. G. Wood, J. Phys. C **16**, 5127 (1983).

[26]See Table S1 in supplementary material at http://dx.doi.org/10.1063/1.4822270 for Bi-O bond lengths in the relaxed ts-BiVO$_4$ and ms-BiVO$_4$ slabs, together with the corresponding bulk values for comparison, and Figure S1 for the complete slab structure employed in this work.

[27]R. M. Hazen and J. W. E. Mariathasan, Science **216**, 991 (1982).

[28]M. W. Stoltzfus, P. M. Woodward, R. Seshadri, J.-H. Klepeis, and B. Bursten, Inorg. Chem. **46**, 3839 (2007).

[29]A. Walsh, D. J. Payne, R. G. Egdell, and G. W. Watson, Chem. Soc. Rev. **40**, 4455 (2011).

[30]C. Franchini, G. Kresse, and R. Podloucky, Phys. Rev. Lett. **102**, 256402 (2009).